Study on Ionospheric Effects on SAR and their Statistics

Giorgio Gomba[a], Francesco De Zan[a], Björn Rommen[b], and Raul Orus Perez[b]
[a]German Aerospace Center (DLR), Münchenerstr. 20, 82234 Weßling
[b]ESA/ESTEC, The Netherlands

Abstract

The objective of this work is to study the impact of ionospheric disturbances on the Sentinel-1 mission. First we realize an ionospheric statistics database based on global TEC models and maps. Then we process interferometric stacks of Sentinel-1 images using the split-spectrum method to estimate the differential ionosphere and validate the GNSS based statistics. We use the newly developed database to determine the expected average and maximum ionospheric errors on Sentinel-1 SAR measurements. We discuss the possibility to routinely include flags or corrections for ionospheric disturbances in Sentinel-1 products.

1 Introduction

This document summarizes the results of the DLR-ESA "Study on Ionospheric Effects on SAR and their Statistics" project. The objective of this activity was to study the impact of ionospheric disturbances on the Sentinel-1 mission. This main objective has been achieved through the realization of an ionosphere statistics database based on global TEC maps, validated and enhanced with real SAR measurements. The average and maximum errors that can be expected on Sentinel-1 SAR measurements have been determined using the newly developed database. Concepts for a flagging method to identify disturbed images, or for correction layers based on different compensation methods have been discussed.

2 Ionospheric Statistics

Global ionosphere maps (GIMs) of vertical electron content (VTEC) distributed by the International GNSS Service (IGS) are one of the source data for this project. They provide an estimation of the ionospheric TEC based on dual-frequency GNSS measurements [1]. They are therefore be more accurate than, for example, models based on climatological parameters. Nevertheless, GIMs spatial resolution is lower than the typical SAR scene size and as a result, small-scale ionospheric variations that affect SAR images are not represented in the global maps.
We used CODE and UHRG TEC maps, based respectively on a global model using spherical harmonics, and on a global voxel-defined 2-layer tomographic model solved with Kriging interpolation. The time spacing of CODE is 2 hours, UHRG is obtained downsampling to one hour the UQRG product which has 15 minutes spacing. Spatial resolution is 5° in longitude and 2.5° in latitude. MAPGPS maps were also included, with respect to the IGS TEC maps, MAPGPS advantages are the higher spatial and temporal resolution and the fact that model fitting or interpolation are not used. For each bin in the grid MAPGPS returns the median of all TEC measurements falling in the bin [2].
The mapping function we used to convert vertical to slant TEC is based on the single layer approximation [3, 4]. We removed the top-side ionosphere, which lies above the radar, by reducing of 30% the TEC value, that is, by considering that only 70% of the total ionosphere is below the satellites. We also tested the Barcelona ionospheric Mapping Function [5], which is meant to be applied in northern mid-latitudes only. However, with respect to using a fixed 0.7 ratio, results showed that the BIMF ratio does not considerably improve the match between GNSS-based statistics and the one derived from SAR measurements. Using a different model or the GNSS receiver on board Sentinel-1 satellites could improve the results and is left for future work.
The geographic grid used in the database is the same as in global ionospheric maps, the temporal sampling of the database is one hour. The database provides yearly averages: the statistics are calculated over a period of one year for the last 6 years of the current solar cycle (2014-2019).
For each grid point the database includes the average, standard deviation, and extremes of the following values:

- Absolute ionosphere: the average TEC level is

$$TEC_{avg} = \langle TEC(n) \rangle \,, \tag{1}$$

  where $\langle\ \rangle$ is the sample average over the samples n. The standard deviation is:

$$\sigma_{TEC} = \sqrt{\langle (TEC(n) - TEC_{avg})^2 \rangle}. \tag{2}$$

- Differential ionosphere: the differential ionosphere standard deviation is: $\sigma_{\Delta TEC} = \sqrt{2}\sigma_{TEC}$
- Absolute ionospheric gradient in range and azimuth: the effective range gradient (measured in TEC/100km) is the gradient in the ionosphere in the

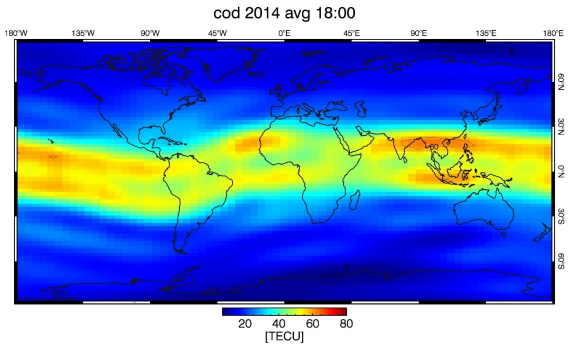

Figure 1 2014 average absolute ionosphere for ascending orbits.

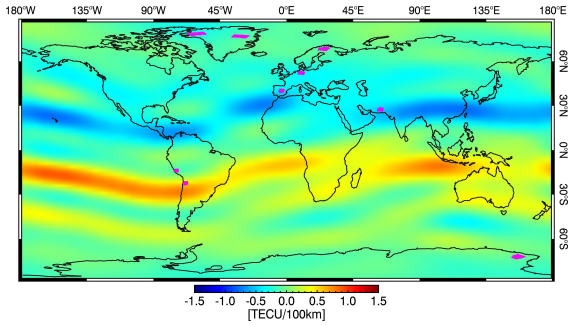

Figure 2 TEC azimuth gradient for ascending images averaged over the period 2017-2019.

range direction plus the absolute ionosphere multiplied by the incidence angle change rate:

$$\partial_{rg}TEC'(n) = (\partial_{rg}TEC(n) + r \cdot TEC(n)) \cdot 100 \cdot 10^3 \quad (3)$$

where

$$r = \frac{M(46°) - M(30°)}{20 \cdot 10^3} / M(38°) \quad (4)$$

using the mapping function M [3, 4] and average Sentinel-1 IW incidence angles and range footprint. In azimuth the gradient is the slope of the TEC map in the along-track direction.

Figure 1 shows an example of the extracted absolute ionosphere, as seen by Sentinel-1 during an ascending orbit in 2014, a solar maximum period. Figure 2 shows an example of the azimuth gradients during ascending orbits averaged over 2017-2019.

3 Statistics Validation

We selected eight sites and at each site both ascending and descending images were used. Site locations are distributed over different ionospheric regions: polar, mid-latitudes, and equatorial. A secondary selection criteria was maximization of interferometric coherence. Figure 2 shows the location of the sites. Stacks of 100 to 300 Sentinel-1 images have been used. The processing was based on three different techniques: interferograms with a single reference image in dry high-coherence equatorial sites, interferograms from PS/DS processing for mid-latitude sites with lower long-term coherence, consecutive interferograms for polar sites with fast ground motion. We applied the split-spectrum method [6] to the interferograms, and saved the gradient of the estimated ionosphere, in the range and azimuth directions, for later analysis.
Figure 3 shows the estimated ionospheric gradients for the ascending Chile stack in the equatorial region. TEC-maps gradients match quite well the SAR-based ones, at least in the range direction, indicating that GIMs estimates well the ionosphere seen by the radar. The mean value of the split-spectrum time series, equivalent to the reference image ionosphere, is removed calibrating it with the GNSS-based time series.

Comparisons of the standard deviations from TEC maps and from split-spectrum gradients show a good match in the range direction. The results are displayed in Figure 4. This suggests that GIMs can be used as a proxy to calculate the expected ionospheric errors. The standard deviation of azimuth gradients from TEC maps are underestimated in Equatorial and Polar regions, with the exception of MAPGPS statistics which present a better match. This could be caused by the smooth ionospheric models which are applied to GNSS data when generating global ionospheric maps. Since MAPGPS is not based on models it is reasonable that it performs better. MAPGS, however, seems to overestimate the statistics more often, this could be due to insufficient upper ionosphere removal. Moreover, MAPGPS is not continuously covering the whole land mass and it could present more outliers than other systems. The comparison also showed that UHR data performed almost always better than CODE and should therefore be preferred.

4 Statistics of Expected Errors

Based on the ionospheric statistics database this section reports to what degree Sentinel-1 data is affected by ionospheric effects. The report is focused on the following errors:

- Positioning error (SAR): this affects ground range and azimuth geolocation positioning of single SAR images.
- Differential offset error (InSAR): this affects range and azimuth motion offsets (scene-average) between a pair of SAR images, measured with motion-tracking based on amplitude cross-correlation and with enhanced spectral diversity.
- Differential gradient error (InSAR): this affects range motion gradients (in range and azimuth direction) between a pair of SAR images, measured with interferometry and with motion-tracking based on amplitude cross-correlation.
- Deformation velocity error (InSAR stack): this affects range motion velocity estimation from a stack of SAR images, measured with interferometry.

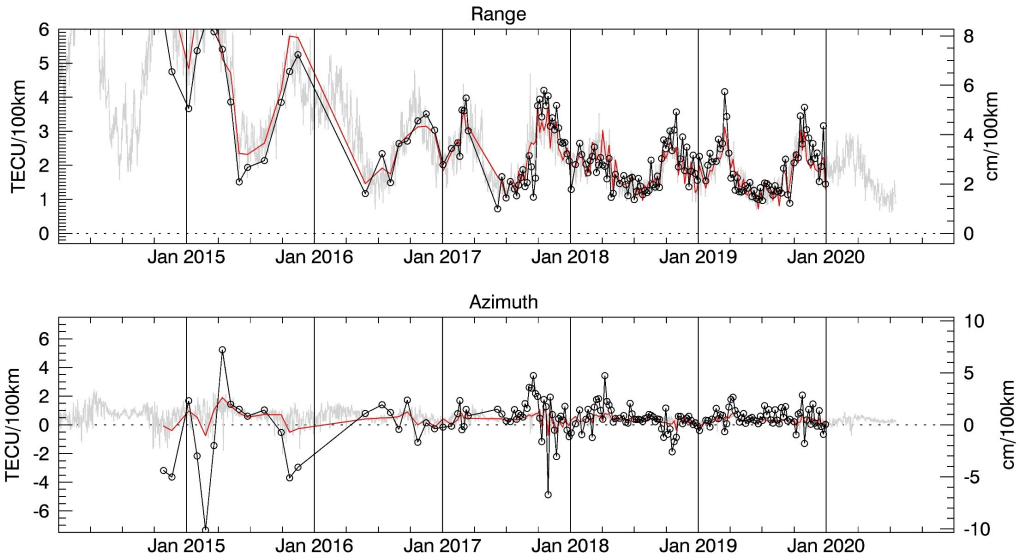

Figure 3 Ionospheric gradients of the ascending Chile stack, estimated using split-spectrum processing. The black dots and the red line are the gradients at the acquisition dates, respectively from SAR and from CODE TEC maps. The gray line represents the CODE TEC maps gradients for all days.

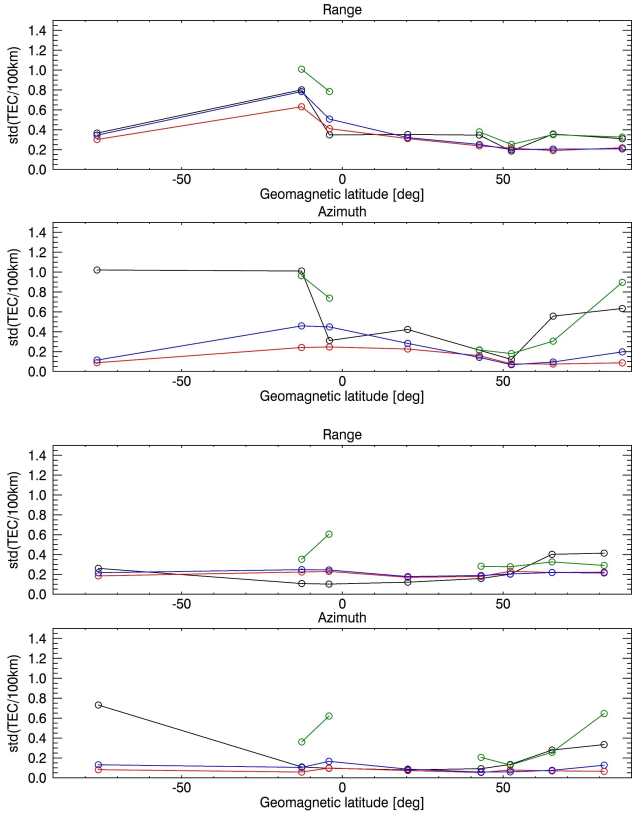

Figure 4 Comparison of the average 2017-2019 ascending (top) and descending (bottom) standard deviations for SAR (black), CODE (red), UHR (blue), and MAPGPS (green).

Table 1 specifies the average and standard deviation values of the expected errors. They are calculated using the ionospheric statistics produced with the UHR TEC global maps. The errors presented in Table 1 are based on global averages and on the complete solar cycle. The following ratios, with respect to the average values in Table 1, can be applied:

- during solar maximum periods errors are 1.75 times bigger;
- during solar minimum periods errors are 1.75 times smaller;
- in mid-latitude areas errors are 1.25 times smaller;
- in equatorial areas errors are 1.61 times bigger in ascending images, and 1.25 times smaller in descending images;
- in polar areas errors are 1.5 times smaller.

Given the statistics validation of the previous section, based on split-spectrum estimations, we can expect the errors in Table 1 to be, in general, a good representation of the true disruption. However, in equatorial and polar regions azimuth errors might be, respectively, 2 and 10 times bigger than what reported in Table 1.

5 Concepts for mitigation strategies in routine operation

This section reports on concepts for a system that shall help the user dealing with ionospheric effects on SAR images. One of the possible solutions is a flagging system. The objective of simple binary flags could be to warn users that an image is so disturbed by the ionosphere that its presence

			ASCE			DESC		
			X	C	L	X	C	L
Position (geolocation)	avg [cm]	gr rg	10.6	33.4	604	5.3	16.8	303
		az	0.7	2.3	41	0.2	0.7	13
Position (geolocation)	std [cm]	gr rg	4.1	12.9	234	2.3	7.2	131
		az	0.9	2.8	51.5	0.5	1.5	27.3
Differential offset (tracking offset)	std [cm]	rg	3.6	11.3	204	2	6.3	114
		az	1.3	4	72.8	0.7	2.1	38.5
Differential gradient (interferogram)	std [cm/100km]	rg	0.4	1.1	20.3	0.2	0.7	12.3
		az	0.2	0.7	12.8	0.1	0.4	6.8
Deformation velocity (stack)	std [mm /100km/year]	rg	0.1	0.3	6.3	0.1	0.2	3.8
		az	0.1	0.2	4	0	0.1	2.1

Table 1 Expected ionospheric errors on SAR and InSAR, derived from UHR TEC maps.

shouldn't be ignored. The user could then discard flagged images to reduce possible problems. The level of disturbances which could be ignored might however depend on the application. Moreover, since the strength of ionospheric effects is geographically different, images marked as disturbed and discarded in a quiet region could be accepted in a more disturbed region. As a result, a single threshold level would be less useful and the user would have no quantitative information about the initial and residual errors. Finally, flags could only be applied to single images since flagging all combination of interferometric pairs would not be possible, reducing the application spectrum of this solution.

Calculable effects could be derived when the expected error level of various ionospheric effects is distributed. The user could then use weights based on the error levels, or avoid images exceeding a threshold selected by the user depending on its objectives. Additionally, initial and residual error levels could be estimated, and if a correction layer is also provided, correction of the errors would be possible.

Supposing to distribute statistics and correction layers based on GIMs it is worth discussing the residual error level that can be expected after corrections. The precision of vertical TEC in global ionospheric maps is assessed to be at worst 4 TECUs in difficult conditions: over the sea and far from receivers. The bias is 1 to a few TECUs. In more generic conditions, the relative error is for most maps between 20% and 30%, meaning that the TEC standard deviation depends on the level of ionosphere: $\sigma_{TEC} = 0.2 \cdot TEC$ [7]. We used the latter to calculate the residual error for the corrections based on absolute TECs. Regarding gradients, we used the split-spectrum estimations to derive the precision of map-based gradients. We defined the difference between the map-based and split-spectrum gradients as the residual after corrections. Results show that the standard deviation of residuals is about 60% and 80% of the original error standard deviation, respectively in range and azimuth, for ascending images.

Operational corrections based on the split-spectrum method and distribution of the results present two main technical difficulties. First the images combination, or interferograms selection, has to be fixed: interferograms with short temporal baselines could be used, but attention should be given in reducing the risk of biases and integration errors. Alternatively, a more computationally intensive phase linking algorithm could be used. Secondly, phase unwrapping could be an issue to operational unsupervised processing. One solution to this problem would be to implement checks on the unwrapped products. Alternatively, the unwrapping could be delegated to the user by delivering only group and (wrapped) phase delay data. This could remove from the user the burden of complex data processing (that is the optimum delays estimation, requiring ESD coregistration, SBAS or phase linking, and split-spectrum) except for phase unwrapping and ionosphere derivation. The latter approach falls in the discussion topic of provision of higher-level products, which would simplify the use of SAR data for users. Finally the feasibility of the approach proposed in [8], which does not require unwrapping the interferogram but only the smooth ionospheric phase, should be evaluated.

6 Conclusion

In this project, using global TEC maps based on GNSS measurements, we created a database of statistics about the variability of the ionosphere and the level of various errors caused to SAR images and interferograms. We validated the statistics and error corrections using ionosphere estimated with the split-spectrum method applied to Sentinel-1 images at various sites. The results shows that TEC maps based statistics are valid for most regions except for azimuth shifts in equatorial and polar images. Finally, we showed that corrections based on global TEC maps can in average reduce the ionospheric error levels.

7 Literature

[1] Roma-Dollase, et al., "Consistency of seven different GNSS global ionospheric mapping techniques during one solar cycle," Journal of Geodesy, 2018.

[2] Rideout, W., Coster, A. "Automated GPS processing for global total electron content data," GPS Solutions 10, 2006.

[3] N. Jakowski, et al., "Total electron content models and their use in ionosphere monitoring".

[4] Y. Xiang et al., “An Enhanced Mapping Function with Ionospheric Varying Height”.

[5] H. Lyu, et al., “The Barcelona ionospheric mapping function (BIMF) and its application to northern mid-latitudes”.

[6] G. Gomba, et al., “Toward Operational Compensation of Ionospheric Effects in SAR Interferograms: The Split-Spectrum Method,” IEEE Transactions on Geoscience and Remote Sensing, 2015.

[7] H. Pajares, et al., “Comparing performances of seven different global VTEC ionospheric models in the IGS context,” in IGS, 2016.

[8] U. Wegmüller, et al. “Reformulating the Split-Spectrum Method to Facilitate the Estimation and Compensation of the Ionospheric Phase in SAR Interferograms,” Procedia Computer Science, Volume 138, 2018.